2,3,5-Tri-O-benzyl-D-xylofuranose

Baptiste Taffoureau, Isabelle Gillaizeau, Pascal Retailleau, Cyril Nicolas

molbank

MDPI

Short Note

2,3,5-*Tri*-*O*-benzyl-D-xylofuranose

Baptiste Taffoureau [1], Isabelle Gillaizeau [1], Pascal Retailleau [2,*] and Cyril Nicolas [1,*]

[1] Institut de Chimie Organique et Analytique (ICOA), UMR 7311 CNRS, Université d'Orléans, Pôle de Chimie, Rue de Chartres, BP 6759, 45067 Orléans CEDEX 2, France; baptiste.taffoureau@sigma-clermont.fr (B.T.); isabelle.gillaizeau@univ-orleans.fr (I.G.)

[2] Institut de Chimie des Substances Naturelles, CNRS UPR 2301, Université Paris-Saclay, 1 Avenue de la Terrasse, 91198 Gif-sur-Yvette CEDEX, France

* Correspondence: pascal.retailleau@cnrs.fr (P.R.); cyril.nicolas@univ-orleans.fr (C.N.); Tel.: +33-(0)-1-69-82-31-19 (P.R.); +33-(0)-2-38-49-26-46 (C.N.)

Abstract: The synthesis and crystallization of 2,3,5-*tri*-*O*-benzyl-D-xylofuranose permitted us to isolate the alpha anomer with a small contamination of the beta form (ca 10%), whose first crystallographic structure obtained in the $P2_12_12_1$ space group was determined at 100 K up to a resolution of sin θ_{max}/λ = 0.71 Å^{-1} and refined to an *R*1 value of 0.0171 with a Hirshfeld atom refinement (HAR) approach.

Keywords: 2,3,5-*tri*-*O*-benzyl-D-xylofuranose; synthesis; Hirshfeld atom refinement of X-ray structure; 3-D Hirshfeld surface; crystal packing

check for updates

Citation: Taffoureau, B.; Gillaizeau, I.; Retailleau, P.; Nicolas, C. 2,3,5-*Tri*-*O*-benzyl-D-xylofuranose. *Molbank* **2022**, *2022*, M1382. https://doi.org/10.3390/M1382

Academic Editor: Kristof Van Hecke

Received: 21 April 2022
Accepted: 1 June 2022
Published: 7 June 2022

1. Introduction

Carbohydrates are ubiquitous key biomolecules that are involved in numerous fundamental biological events. They are an integral part of living cells acting as a vital source of energy, structural building blocks, and cell surface receptors or mediators [1].

Given the pivotal roles of mono-, oligo- and polysaccharides as well as glycoconjugates in the process of life, carbohydrate-mediated processes have therefore progressively been labeled as promising targets in drug discovery [2]. However, sugar derivatives are typically not ideal candidates for therapeutic purposes, as they are mostly unstable and susceptible to hydrolysis [e.g., hemiacetals (aldoses), hemiketals (ketoses) or acetals and ketals (*O*-glycosides)] [2].

As potential drug candidates, carbohydrate mimics have accordingly gained increased interest, because of their ability to modulate the activity of carbohydrate-processing enzymes, while circumventing the enzymatic and chemical instability of sugars in mammals [3–5]. Efforts have thus been devoted to using carbohydrates as synthetic intermediates to generate glycomimetics via chiron approaches.

One class of saccharide analogues that is currently attracting a surge of interest is that of iminosugars. These small molecules, also known as azasugars, are a class of compounds capable of acting as inhibitors or enhancers of many enzymes that act on glycosides, prominently on glycosidases [6–8], and glycosyltransferases [9]. They have become the most popular class of glycomimetics reported to date, being able, for instance, to regulate the folding and transport of glycoproteins (e.g., chaperone effect), to alter the glycosylation profile of eukaryotic cells, to interfere in the carbohydrate and glycoconjugate metabolism, and to stop virus attachment and the infection of host cells [6–8,10,11].

In our ongoing research directed towards iminosugars, we exploited the alpha and beta forms of 2,3,5-*tri*-*O*-benzyl-D-xylofuranose **1** to prepare imino-L-arabinitol-*C*-glycosyl compounds as simplified UDP-Gal*f*-transferase inhibitors [12–17]. Compound **1** was further used by Martin and others, as a surrogate to build analogues of (−)-steviamine [18], (+)-1-azafagomine [19], and radicamines A, and B [20,21], etc. The spectral characterization data of compound **1** (IR, ^{1}H- and ^{13}C-NMR, HRMS) and its *ent*- derivative was described

in [22–24]; however, to our knowledge, the X-ray crystal structures of the enantiomers have not so far been determined. Herein, we report the synthesis of 2,3,5-*tri*-*O*-benzyl-α,β-D-xylofuranose (with a different method, see Section 2.1 below, and experimental part), and the crystallographic description (Ortep structure, 3-D Hirshfeld surface and crystal packing) of 2,3,5-*tri*-*O*-benzyl-D-xylofuranose mixing both anomers.

2. Results and Discussion

2.1. Synthesis

Our investigation commenced from D-xylose, which was converted into 2,3,5-*tri*-*O*-benzyl-α,β-D-xylofuranose **1** in 29% overall yield over three steps with only one purification (Scheme 1). Following typical conditions, D-xylose was inserted in a mixture of dry methanol and acetyl chloride, and the reaction mixture was heated at 30 °C for 3.5 h. The crude mixture was neutralized by addition of a basic resin. Compound **2** was then reacted with an excess of benzyl bromide and NaH in DMF at 20 °C for 20 h to afford methyl 2,3,5-*tri*-*O*-benzyl-α,β-D-xylofuranoside **3**. Compound **1** (α/β ca. 2:3, $CDCl_3$ solution, 25 °C) was obtained through subsequent hydrolysis by treatment with a mixture of glacial acetic acid and 1 M aq. HCl solution at 80 °C for 17 h, followed by 4 h at 100 °C.

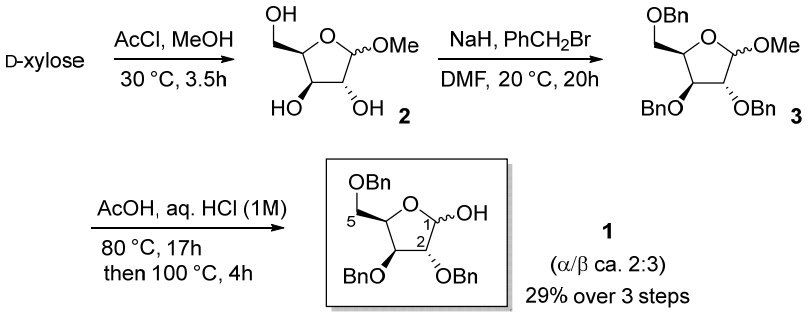

Scheme 1. Synthesis of 2,3,5-*tri*-*O*-benzyl-α,β-D-xylofuranose.

2.2. Structural Commentary

The structure of D-xylofuranose **1** was confirmed beyond doubt by single crystal X-ray diffraction studies performed upon crystals belonging to non-centrosymmetric Sohncke space group, $P2_12_12_1$, at the Mo Kα radiation and at low temperature (100 K) with refined Flack parameter close to 0. Additional redundant measurements on a copper source but at room temperature and limited to a resolution of $(\sin\theta/\lambda) = 0.6$ Å^{-1} confirmed the significance of the Flack parameter in line with the starting D-xylose derivative.

The molecule found to occupy the asymmetric unit consists of a furanose ring substituted by two O-benzyl groups at C2 and C3, one Met-OBn group in position 4 and one hydroxyl group in position 1. Completion of the independent atom model (IAM) refinement with all hydrogen atoms constrained to geometric positions suggested slight disorder of the central O-benzyl group at C3 treated as static over two close sites and the hydroxy group at C1 in an equatorial position. Nevertheless, at that stage, the first residual peak in the Fourier difference synthesis—albeit low (<0.3e.Å^3) but almost twice the value of the second peak—was located in the axial position of C1 in the vicinity of the disordered O-benzyl group. The possibility that the two anomeric forms could be present inside the crystal was therefore checked. We ended up with the confirmation that crystallization of the neat mixture of alpha and beta anomers (unknown ratio) trapped the α-form in large majority over the β form (ca. 0.89(1):0.11(1)). Carbohydrate hemiacetals can obviously exist in two anomeric isoforms, either in the solid or liquid state. In the case of compound **1**, the α anomer is heavily favored in the crystal state, whereas in $CDCl_3$ at 25 °C, the equilibrium is shifted towards the β form. One may therefore advocate for the selective crystallization of the α- over the β-anomer (e.g., optical resolution). However, there is no evidence that the neat amorphous solid did not already contain the two forms in an α/β ratio of 89:11, and its dissolution in $CDCl_3$ slowly shifted the mutarotation

equilibrium towards a ca. 2:3 ratio in favor of the β form. Further diffraction measurement at low temperature and at extended resolution allowed us to perform a Hirshfeld atom refinement (HAR) to document in greater detail the structural parameters of **1** including those of the H atoms (Figures 1, 2, and 5, plus Tables 1–3, and Figure S1 and Table S1 in the supporting information (SI)).

The furanose group flexibility was found uncorrelated to the disorder of the central O-Bn group, a disorder that could be considered as essentially dynamic. While the major α form can be seen to be stabilized by an intramolecular hydrogen bond with O2, graph-set symbol S(5), (see Table 2) and benefit from developing a weak intermolecular H-bond (see below Figure 1, and crystal packing analysis in Figure 4), the minor β-form can find in O3 a 'lifeline' in a hydrophobic environment to make an intramolecular h-bond (graph-set, symbol S(6)).

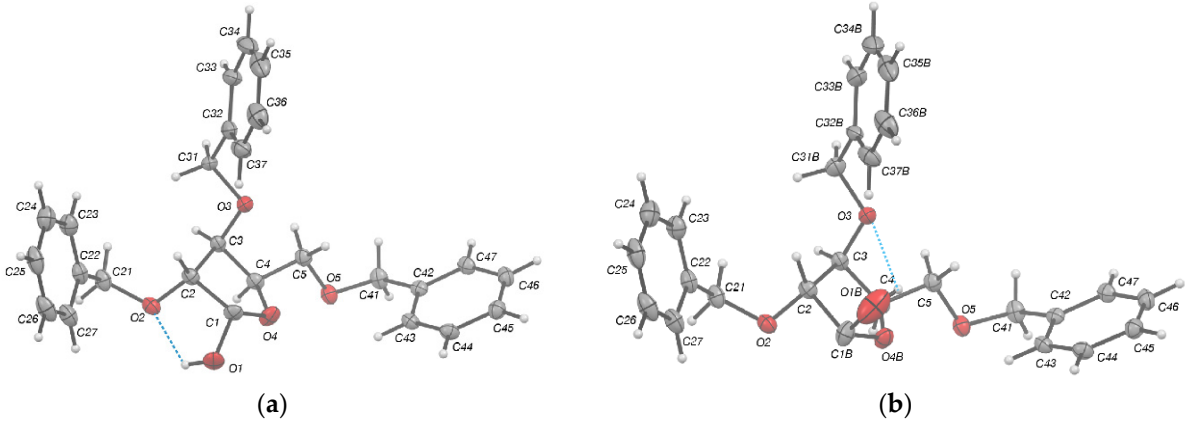

(**a**) (**b**)

Figure 1. (**a**) Molecular structure of (α)-**1** with numbering scheme and anisotropic displacement ellipsoids drawn at the 50% probability level, hydrogen atoms being represented by spheres of arbitrary radius; (**b**) Ortep view of the minor (β)-**1** compound. Dotted line in cyan highlights the intramolecular h-bond.

The conformational analysis of the furanose ring (Figure 2) based on its internal dihedral angles and its deviation from planarity showed that the pseudorotational phase angle $P \cong 11^\circ$ and the maximum puckering amplitude $\nu_{max} \cong 35$ (see Table 1) [25,26]. Thus, this ring adopts a conformation close to $^3T_2$, where C2 and C3 deviate by 0.116 and −0.443 Å, (by 0.467 and −0.058), respectively, from the plane through atoms C1(B)/C4/O4(B).

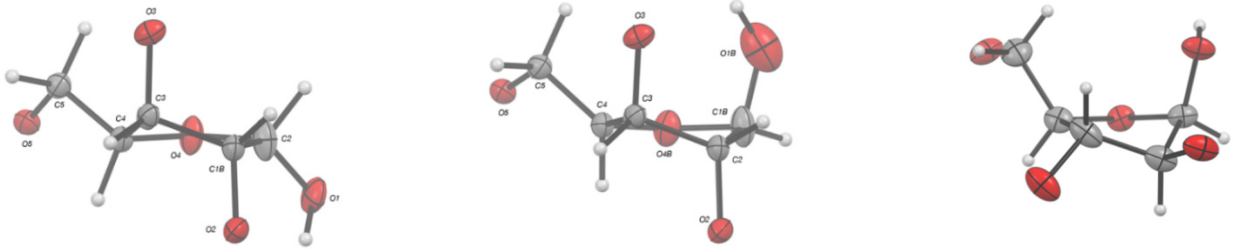

(**a**) (**b**) (**c**)

Figure 2. Close-up of the sugar ring puckering C3-endo, C2-exo (N-type) conformations for the (**a**) α form, and (**b**) β form. (**c**) Conformation of the 2,3,5-*tri*-*O*-benzyl-β-D-arabinofuranose analogue, depicted in the CCDC Refcode: LUHROX.

A search in the Cambridge Structural Database (CSD, [27]) revealed the structure of a homologous compound (CCDC Refcode: LUHROX, [28]) which is the 2,3,5-*tri*-*O*-benzyl-β-D-arabinofuranose (see Figure 2c) whose geometric parameters are listed in Table 2 for comparison. The torsion angles of (α,β)-**1**, C2—O2—C21—C22 = −69.10 (6)° and C5—O5—

C41—C42 = 83.03(6)° are *gauche*, meaning that the two opposite substituents are not fully extended, bringing the respective centroids of the phenyl rings to a distance of 11.1 Å (2Å shorter than in the conformers of the homologous structure, LUHROX). Altogether with the O-benzyl group axially positioned at C3 with the ring overhanging orthogonally the furanose, the overall conformation adopted inside the crystal features a folding or closing trend for a 'three petal flower', conversely to the 'open' homologous structure.

Table 1. Hydrogen bonds [Å and °] [1].

D—H...A	d(D—H)	d(H...A)	d(D...A)	<(DHA)
O1—H1...O2	0.964(10)	1.938(11)	2.5739(7)	121.3(8)
O1—H1...O5 #1	0.964(10)	2.548(10)	3.3601(7)	142.0(8)
O1B—H1B...O3	0.964(10)	2.299(11)	2.9095(7)	120.4(8)
C23—H23...O1 #2	1.010(7)	2.299(11)	3.1929(7)	158.84(8)
C27—H27...O5 #1	1.084(8) [1]	2.3889(11) [1]	3.4537(7)	166.88(8)

[1] Symmetry transformations used to generate equivalent atoms: #1 1−x, 1/2+y, 3/2−z; #2 x−1, y, z.

Table 2. Geometrical parameters of the torsion angles (°) and pseudorotation parameters (°) of the furanose ring for the two coexisting anomers (I) and molecules A and B of D-arabinofuranose hemiacetal analogue [25].

Torsion Angle	(α)-I	(β)-I	Molecule A [(4)]	Molecule B [(4)]
C4—*O4*—*C1*—C2	4.55 (11)	17.4 (10)	32.47 (3)	33.58 (3)
O4—*C1*—C2—C3	−24.39 (13)	−29.29 (12)	41.02 (3)	41.29 (3)
C1—C2—C3—C4	33.41 (7)	32.07 (11)	34.19 (3)	33.51 (3)
C1—*O4*—C4—C3	17.55 (9)	2.2 (6)	15.85 (3)	13.88 (3)
C2—C3—C4—*O4*	−32.07 (10)	−21.6 (8)	10.74 (3)	−13.07 (3)
H1—*O1*—*C1*—*O4*	−99.8 (6)	67.17 (8)	−54.2 (3)	−66.8
X [(1)]	*syn*	*syn*	*syn*	*syn*
C3—C4—C5—O5	−167.42 (5)	−167.42 (5)	−172.2 (3)	−173.8
$\gamma^t/\gamma^+/\gamma^-$ [(2)]	γ^t	γ^t	γ^t	γ^t
Phase angle (P)	11.1 (2)	13.5(17)	327.3	324.4
Puckering amplitude (ν_{max})	35.0 (1)	32.6 (7)	41.3	41.6
S or N [(3)]	N	N	N	N

[(1)] For *anti*, $\chi = 180 \pm 90°$, and for *syn*, $\chi = 0 \pm 90°$. [(2)] $\gamma^t = 180°$, $\gamma^+ = 60°$ and $\gamma^- = -60°$. [(3)] For south S-type, $P = 180 \pm 90°$, and for north N-type, $P = 0 \pm 90°$. [(4)] Data for molecules A and B of compound **1** homologous molecules were retrieved from the CSD (Refcode: LUHROX).

Inside the crystal (α,β)-**1**, the molecules spiral around the 2-fold screw axis at 0,y, $\frac{1}{4}$ and $\frac{1}{2}$,y,$\frac{3}{4}$ in antidromic infinite chains, **C** (7), via distant H-bond interactions between the hydroxy O1 donor and O5 of the Met-OBn chain of the vicinal molecule at the position #1 1−x, y+1/2, 3/2−z (d O1(–H1)···O5$^{\#1}$ = 3.360Å, ∠ (O1–H1···O5$^{\#1}$) = 142.0°), interactions reinforced by shorter non-conventional H-bonds between C27 and O5 (d C27(–H27)···O5$^{\#1}$= 3.454 Å, ∠ (C27–H27···O5$^{\#1}$) = 166.9°), and also C23 and O1 at #2 x−1, y, z (d C23(–H23)···O1$^{\#2}$ = 3.193 Å, ∠ (C23–H23···O1$^{\#2}$) = 158.8°). These are the specific points of contact in the crystal which appear as red spots on the largely blue Hirshfeld surface of (α,β)-**1** (Figure 3) [29].

The molecular packing of (α/β)-**1** features along the **ab** plane 'hydrophilic' and 'hydrophobic' layers containing the benzyl groups with some disorder and whose most noticeable interaction is C45–H45 · · · π(*Cg*4)$^{\#3}$ (*Cg*4 referring to the centroid of the C42/C47 phenyl ring at position #3: x+$\frac{1}{2}$, $\frac{1}{2}$−y, 1−z, d H45···*Cg*4$^{\#3}$ = 2.563(1)Å, ∠ (C45–H45···*Cg*4)$^{\#3}$) = 151.4°) (Figure 4a). Analysis of the Hirshfeld surface indicated that this type of interaction (C···H/H···C) accounted for a fourth of the contact contribution of the overall surface, which is more than twice the (O···H/H···O) contribution, but exceeds the van der Waals interactions by 61.9 %. The same ratios can be observed for LUHROX although its molecular assembly differs with molecules A and B, of the asu, making h-bonded interactions via the O1–H1···O4 h-bonds between their central furanose rings, the chained dimers piling up in columns along the ***a*** direction of its monoclinic, P 2_1, unit cell (Figure 4b).

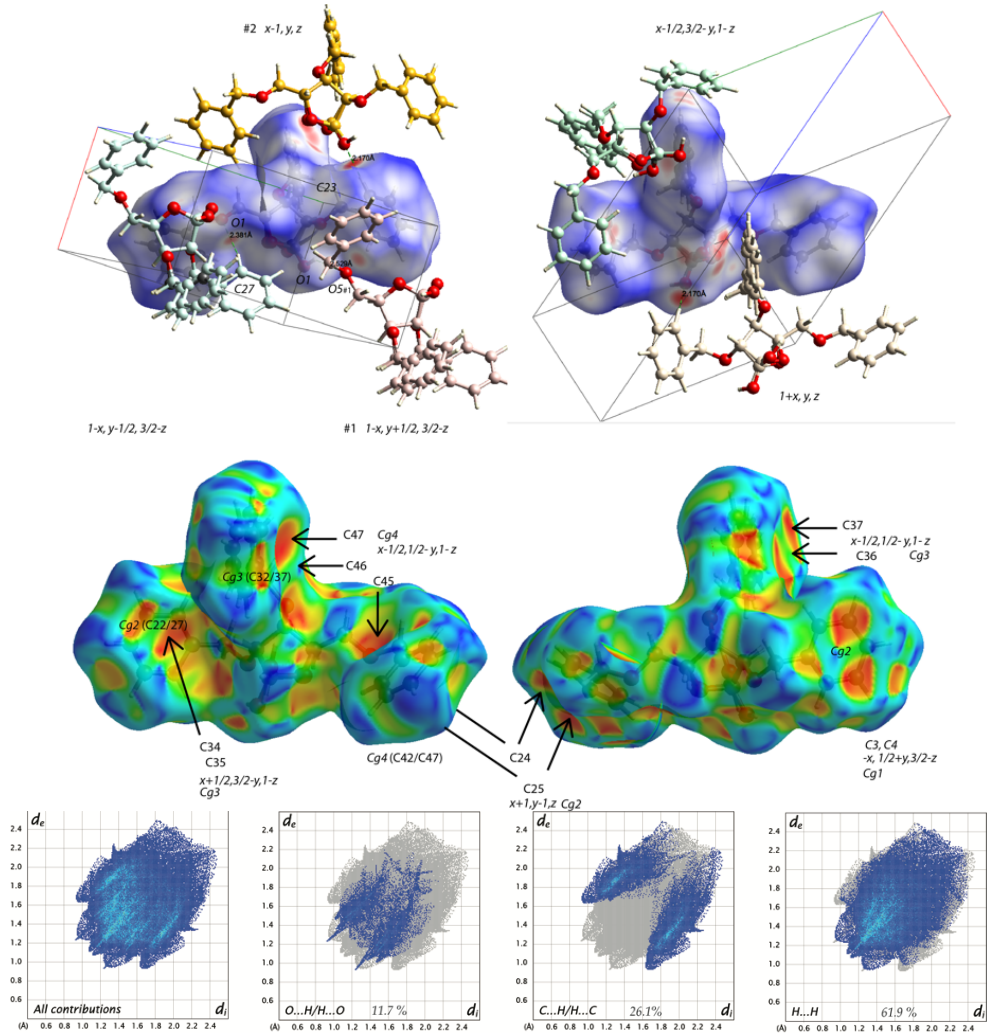

Figure 3. (**Top**) views of the 3-D Hirshfeld surface plotted over d_{norm} in the range from −0.3365 to 1.1653 a.u, (**Middle**) over the shape-index property highlighting C–H . . . π interactions and (**Below**) the 2-D fingerprint plots of the mixture of D- showing close contacts of all contributions in the crystal and those delineated into the three main types of interactions. d_{i} and d_{e} denote the closest internal and external distances in Å from a point on the surface.

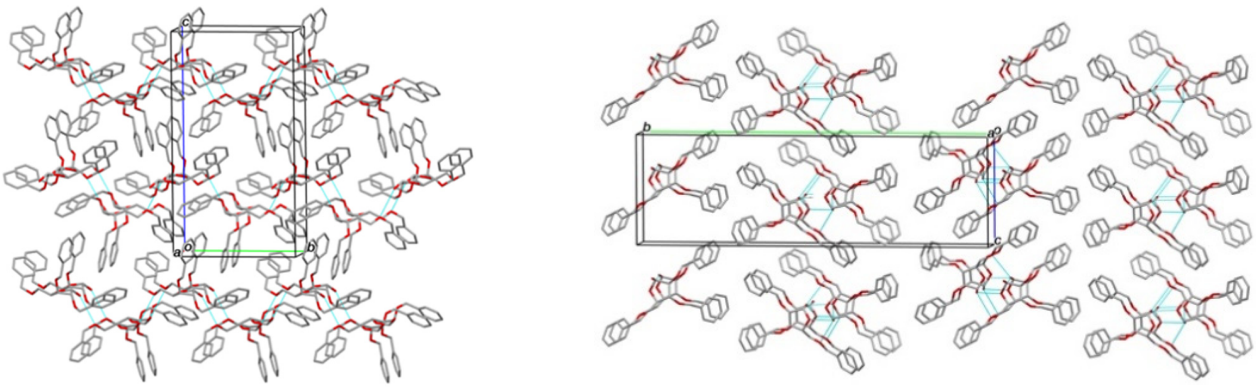

(**a**) (**b**)

Figure 4. (**a**) Partial view of the crystal packing of (α,β)-**1** (ca. 89:11) along the ***a*** axis. O-H···O hydrogen bonds are shown as cyan dotted lines; (**b**) for comparison, a view of the LUHROX packing along the ***a*** axis, also highlighting the extended conformation of the homologous molecule is reported.

3. Materials and Methods

3.1. General Remarks

Unless otherwise stated, all reagents and starting materials were purchased from commercial sources and used as received. Methanol (anhydrous, 99.8%) was purchased from Sigma-Aldrich Chimie S.a.r.l—38297 Saint-Quentin-Fallavier CEDEX, France. *N*,*N*-Dimethylformamide (ACS reagent, ≥99.8%) was purified by passage through a column containing activated alumina under nitrogen pressure (Dry Solvent Station GT S100, Glass Technology, Geneva, CH). Amberlite®IRA-400 was prepared in its OH^- form by passing 1 M KOH until the effluent was free of chloride ions, it was then washed with distilled H_2O until neutral and then with MeOH. NMR spectra were recorded at 298 K with a Bruker Avance III HD nanobay 400 MHz spectrometer equipped with a BBO probe—Brucker France S.A.S., 67166 Wissembourg CEDEX. The structure of compound **1** (α/β ca. 2:3, $CDCl_3$ solution) was assigned with the aid of 1 D [^{1}H NMR, ^{13}C NMR, Distortionless Enhancement by Polarization Transfer (DEPT)] and 2 D Correlation Spectroscopy [(1H−1H COSY, and ^{1}H−^{13}C Heteronuclear Single Quantum Coherence (HSQC)] experiments. ^{1}H NMR (400 MHz) chemical shift values are listed in parts per million (ppm), relative to the corresponding nondeuterated solvent. Data are reported as follows: chemical shift (ppm on the δ scale), multiplicity (s = singlet, d = doublet, and po = partially overlapped), coupling constant *J* (Hz), and integration. Acquisition of the ^{13}C NMR (101 MHz) spectrum of compound **1** (α/β ca. 2:3, $CDCl_3$ solution) was performed on a broad-band decoupled mode. Chemical shift values are given in ppm, and are related to the corresponding non-deuterated solvent. High-resolution mass spectra were recorded with a Bruker maXis ESI qTOF ultrahigh-resolution mass spectrometer coupled to a Dionex Ultimate 3000 RSLC system. MS data were acquired in positive mode and were processed using Data Analysis 4.4 software (Bruker). The infrared spectrum of compound (α,β)-**1** was recorded neat with a Thermo Scientific Nicolet IS10 FTIR spectrometer using diamond ATR golden gate sampling (Thermo Fisher Scientific, 28199 Bremen, Germany), and is reported in wave numbers (cm^{-1}). Analytical thin-layer chromatography (TLC) was performed with Merck Silica Gel 60 F254 precoated plates—VWR Avantor, F-93114 Rosny-sous-Bois CEDEX, France. Visualization of the developed chromatogram was performed under ultraviolet light (254 nm) and on staining by immersion in aqueous, acidic ceric ammonium molybdate followed by charring at ca. 150 °C. Column chromatography was performed in air on Silica Gel 60 (230–400 mesh) with petroleum ether (bp 40–65 °C) and ethyl acetate (EtOAc) as eluents. Organic solutions were concentrated under reduced pressure with a Büchi rotary evaporator—BÜCHI SARL, 91140 Villebon-sur-Yvette, France. Conformation, crystal packing and geometrical parameters for the LUHROX D-arabinofuranose hemiacetal analogue were obtained from the Cambridge Structural Database (CSD, Version 5.42; Nov 2021, Cambridge, UK [27]). Hirshfeld surface of (α,β)-**1** was drawn using *CrystalExplorer 17.5-f4e298a*, University of Western, Australia [29]. X-ray structure determination at *rt* and 100K was performed on a Rigaku rotating anode—ELEXIENCE SA, 91371 Verrières-le-Buisson CEDEX, France. X-ray data were then processed using *CrystalClear 2.0*, Tokyo, Japan [30] or *CrysAlisPro 1.171.41.121a*, Yarnton, UK [31]. In both cases, the structure was solved by intrinsic phasing methods (*SHELXT Version 2018/2*, University of Göttingen, Germany [32]). Refinement was done subsequently by full-matrix least-squares against F^2 (*SHELXL Version 2018/3*, University of Göttingen, Germany) [33]). Ultimately, it was pursued with the Hirshfeld atom refinement (HAR; [34]) with the *NoSpherA2* [35] implementation in *OLEX2-1.5*, Durham University, UK [36]. Bijvoet analyses were performed with *Platon* (*version170914*, Utrecht University, The Netherlands).

3.2. Procedures and Characterization Data

3.2.1. Synthesis of 2,3,5-*Tri-O*-benzyl-α,β-D-xylofuranose (α,β)-**1**

A single-necked round-bottomed flask under argon atmosphere was charged with AcCl (2.5 mL, ca. 35.0 mmol) and dry MeOH (300 mL), and the solution was stirred at 20 °C for 30 min. D-xylose (5.0 g, 33.3 mmol) was then added and the reaction mixture

was stirred for 3.5 h at 30 °C. Resin Amberlite IRA-400 (OH^- form) was added until pH 8, and the solution was filtered through a cotton plug and concentrated under vacuum. The crude product (R*f* 0.6; SiO_2, CH_2Cl_2/MeOH 8:2, *v*/*v*) was obtained as a light-yellow oil, and used in the next step without further purification.

To the just-generated methyl α,β-D-xylofuranoside (**2**) under argon atmosphere, cooled to 0 °C with an ice water bath, were successively added anhydrous DMF (100 mL) and NaH (60% dispersion in mineral oil, 8.0 g, 200.0 mmol) portionwise; the resulting suspension was stirred continuously at the same temperature for 30 min. Benzyl bromide (17.0 mL, 143.0 mmol) was then added dropwise, and the reaction mixture was allowed to reach room temperature. Stirring was pursued for 20 h and the temperature was adjusted to 0 °C (ice water bath). Water (50 mL) was added, dropwise, and the aqueous phase was extracted twice, with Et_2O (2 × 150 mL). Next, combined organic layers were washed with H_2O (100 mL), sat. aq. $NaHCO_3$ (100 mL) and brine (100 mL). The organic phase was dried ($MgSO_4$), filtered over a cotton plug and the solvent was removed by rotary evaporation.

A single-necked round-bottomed flask under air atmosphere was charged with the mixture of α and β-anomers of 2,3,5-*Tri-O*-benzyl-α,β-D-xylofuranoside (**3**) [R*f* 0.4 (β anomer), R*f* 0.2 (α anomer); SiO_2, petroleum ether/EtOAc 9:1, *v*/*v*], glacial acetic acid (63 mL, ca. 1.1 mol) and aq. HCl (1 M, 16 mL, ca. 0.58 mol) and the solution mixture was heated for 17 h at 80 °C and 4 h at 100 °C. The mixture was allowed to reach room temperature and the solution was neutralized by addition of a 5 M aq. solution of KOH (5 M). The aqueous phase was extracted with EtOAc (2 × 150 mL) and the combined organic layers were washed with H_2O (100 mL), aq. sat. $NaHCO_3$ (100 mL) and aq. sat. NaCl (100 mL). The organic phase was dried ($MgSO_4$), filtered over a cotton plug and the solvent was removed through rotary evaporation. The crude product was purified by column chromatography (SiO_2, petroleum ether/EtOAc 8:2, *v*/*v*) to give **1** as a colorless syrup (4.1 g, 29.3% over three steps).

Mixture of anomers (α/β ca. 2:3, $CDCl_3$ solution, 25 °C). R*f* 0.2 (SiO_2, petroleum ether/EtOAc 8:2, *v*/*v*). ^{1}H NMR (400 MHz, $CDCl_3$): δ 7.58–7.33 (po, 15H, H_{Ar}), 5.65 (br d, $^3J_{1',2}$ 4.2 Hz, 0.4H, H-1α), 5.46 (br s, 0.6H, H-1β), 4.84–4.50 (po, 7H, 3 × OCH_2Phα, 3 × OCH_2Phβ, H-4α, H-4β), 4.49–4.26 (po, 1H, OHα, OHβ), 4.26 (dd, $^3J_{3',4}$ 5.5 Hz, $^3J_{2',3}$ 3.1 Hz, 0.6H, H-3β), 4.23 (dd, $^3J_{3',4}$ 4.7 Hz, $^3J_{2',3}$ 2.7 Hz, 0.4H, H-3α), 4.18 (br dd, $^3J_{2',3}$ 3.1 Hz, $^3J_{1',2}$ 0.8 Hz, 0.6H, H-2β), 4.10 (dd, $^3J_{1',2}$ 4.2 Hz, $^3J_{2',3}$ 2.7 Hz, 0.4H, H2α), 3.98–3.78 (po, 2H, H-5, H-5′) ppm. ^{13}C NMR (101 MHz, $CDCl_3$): δ 138.1 (C, C_{Ar}α), 137.7 (C, C_{Ar}α), 137.5 (C, C_{Ar}β), 137.4 (C, C_{Ar}β), 137.3 (C, C_{Ar}β), 136.9 (C, C_{Ar}α), 128.4–127.7 (CH, CH_{Ar}α, CH_{Ar}β), 101.6 (CH, C-1β), 95.9 (CH, C-1α), 86.5 (CH, C-2β), 81.4 (CH, C-2α), 81.2 (CH, C-3β), 81.0 (CH, C-3α), 79.6 (CH, C-4β), 77.0 (CH, C-4α), 73.4 (CH_2, OCH_2Phβ), 73.3 (CH_2, OCH_2Phα), 72.7 (CH_2, OCH_2Phα), 72.4 (CH_2, OCH_2Phβ), 72.1 (CH_2, OCH_2Phα), 71.6 (CH_2, OCH_2Phβ), 68.7 (CH_2, C-5β), 68.3 (CH_2, C5α) ppm. IR (neat): $\tilde{\nu}$ = 3419 (O–H), 3030 (C–H $_{Ar}$), 2886 (C–H), 1454 (C=C), 1056 (C–O), 735 (C–H $_{Ar}$), 696 (C–H $_{Ar}$) cm^{-1}. HRMS (ESI): *m*/*z* calcd. for $C_{26}H_{28}NaO_5$ $[M + Na]^+$ 443.1826, found 443.1826.

3.2.2. Crystallization of 2,3,5-*Tri-O*-benzyl-α,β-D-xylofuranose (α,β)-**1** (ca. 89:11)

Single crystals of (α,β)-**1** (ca. 89:11) were grown by standing the crude mixture of 2,3,5-*tri-O*-benzyl-D-xylofuranose at 4 °C for 3 days. Massive colorless blocks showed up covering part of the inner walls of the balloon. X-ray structure determination was carried out by collecting diffraction data first at room temperature (*rt*) on a Rigaku rotating anode using microfocused Cu Kα radiation λ = 1.54187 Å (Table S1, see SI), then after cooling the crystal down to 100K using microfocused Mo Kα radiation λ = 0.71073 Å. Crystal data, data collection and structure refinement details are summarized in Table 3 (see below). X-ray data were processed using *CrystalClear 2.0* [30] or *CrysAlisPro 1.171.41.121a* [31], respectively. In both cases, the structure was solved by intrinsic phasing methods (*SHELXT* Version 2018/2 [32]). Its refinement was done subsequently by full-matrix least-squares against F^2 (*SHELXL* Version 2018/3 [33]), with hydrogen atoms constrained to idealized geometries and riding isotropic displacement parameters for the *rt* (sinθ/λ = 0.6 Å^{-1})

dataset, or freely refined with some distance restraints for the 100K ($\sin\theta/\lambda$ = 0.7 Å^{-1}) dataset. Ultimately, it was tentatively pursued further with the Hirshfeld atom refinement (HAR; [34]) with the *NoSpherA2* [35] implementation in *OLEX2-1.5* [36], *using* B3YLP DFT functional [37] and basis set def2-SVP [38] accounting for the non-spherical nature of the electron distribution, which helped us to remove density residuals lying along the covalent bonding (Figure 5). Most H atoms were refined anisotropically and independently except certain H atoms in disordered parts, and refractory to ISOR (*SHELXL*) restraint benefits. The disordered O3-bonded benzyl group with restraints upon 1,2 (sd 0.01) and 1,3 (sd 0.04) distances similar to those in the benzyl group bonded to O5 was refined over two static sites with an occupancy ratio of 0.54(1):0.46(1). The small electronic density residual around the C1 position could be interpreted as potential coexistence of alpha/beta anomers inside the crystal with a ratio refined to 88.7(2):11.3(2). This almost anecdotical mixture did not harm the significance of the 'double-checked' Flack absolute structure parameter [39] in favor of ($_{(0.89)}$*2S*:$_{(0.11)}$*2R,3R,4S,5R*)-3,4-bis(benzyloxy)-5-((benzyloxy)methyl)tetrahydrofuran-2-ol and consistent with the known configuration of the D-xylose starting material. The HAR Crystal structure was deposited at the Cambridge Crystallographic Data Centre as CCDC 2150903 [40]. The data can be obtained free of charge from the CCDC via http://www.ccdc.cam.ac.uk/getstructures (or from the CCDC, 12 Union Road, Cambridge CB2 1EZ, UK; Fax: +44 1223 336033; E-mail: deposit@ccdc.cam.ac.uk).

Table 3. Crystal data, data collection and structure refinement details of compound **1**.

Identification code		2,3,5-*Tri-O*-benzyl-α-D-xylofuranose (α,β)-**1** (89:11)	
Empirical formula, (weight)		$C_{26}H_{28}O_5$, (420.48)	
Temperature (K)		100(2)	
Diffractometer Rigaku®		XtaLabPro mm003+Pilatus200k	
Wavelength (Å)		0.71073	
Crystal system, space group		$P2_12_12_1$, Orthorhombic	
Unit cell dimensions (Å, α = β = γ = 90°)		a = 6.9002(1) b = 13.1783(2) c = 23.9751(5)	
Volume (Å^3)		2180.13(6)	
Z, Calculated density (Mg/m^3)		4, 1.281	
Absorption coefficient (mm^{-1})		0.088	
F(000)		896	
Theta range for data collection (°)		2.98 to 30.25	
Limiting indices		$-9 \leq h \leq 9$, $-17 \leq k \leq 18$, $-33 \leq l \leq 33$	
Reflections collected/unique		55,919/6102	
R(int)		0.0370	
Completeness to $\theta_{max\ (iUCR)}$ (%)		99.8	
Absorption correction method		Gaussian and Multi-scan	
Max. and min. transmission		1.000 and 0.302	
Refinement method		IAM *Shelxl*	HAR *NoSpherA2*
Data/restraints/parameters		6102/416/419	6102/484/693
Goodness-of-fit on F^2		1.028	1.1284
Final R indices [$I > 2\sigma(I)$]	*R1*, *wR2*	0.0338, 0.0896	0.0171, 0.0305
R indices (all data)	*R1*, *wR2*	0.0352, 0.0903	0.0185, 0.0307
Absolute structure parameter [39]		−0.02(15)	0.07(14)
Largest diff. peak and hole (e.Å^{-3})		0.273 and −0.192	0.145 and −0.124

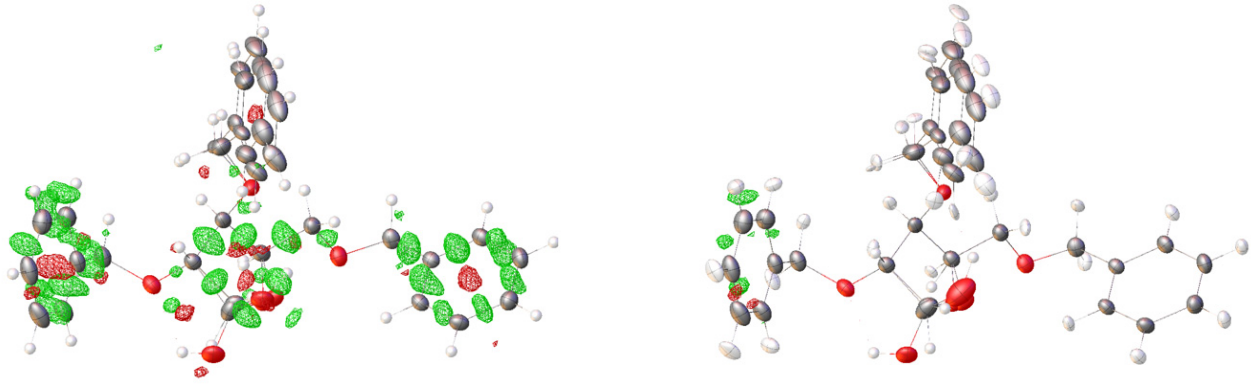

(**a**) (**b**)

Figure 5. Wire visualizations of the residual electron density maps over the molecular structure of compound **1** after (**a**) IAM and (**b**) HAR refinement. The residual density was calculated with *Olex2* Ofrom fcf files and plotted on a grid of 0.05 Å with an iso-value of 0.121 eÅ^{-3} (0.10 eÅ^{-3}, respectively) (green = positive, red = negative).

Supplementary Materials: The following are available online, Table S1: Experimental details for XRD performed at room temperature using copper radiation, Figure S1: Bijvoet pair analyses to assess the absolute configuration of compound **1** (α/β ca. 89:11), Figure S2: ^{1}H NMR (400 MHz, $CDCl_3$) spectrum of compound **1** (α/β ca. 2:3), Figure S3: ^{13}C NMR (101 MHz, $CDCl_3$) spectrum of compound **1** (α/β ca. 2:3).

Author Contributions: Conceptualization, C.N.; funding acquisition, I.G.; synthetic methodology, B.T.; NMR analysis, C.N.; X-ray collection and structure solving, P.R.; writing—original draft, review and editing, P.R. and C.N. All authors have read and agreed to the published version of the manuscript.

Funding: This research was funded by the CNRS (Centre National de la Recherche Scientifique).

Data Availability Statement: The X-ray data are available at CCDC under ref. code CCDC 2150903.

Acknowledgments: The authors are grateful for financial support from the LABEX SynOrg (ANR-11-LABX-0029), and IRON (ANR-11-LABX-0018-01), Techsab (FEDER-FSE 2014-2020-EX011313), and the ARD BIOMEDICAMENT.

Conflicts of Interest: The authors declare no conflict of interest.

References

1. Ernst, B.; Hart, G.W.; Sinaÿ, P. (Eds.) *Carbohydrates in Chemistry and Biology*; Wiley-VCH: Weinheim, Germany, 2000.
2. Tiwari, V.K. (Ed.) *Carbohydrates in Drug Discovery and Development: Synthesis and Application*, 1st ed.; Elsevier: Amsterdam, The Netherlands, 2020; ISBN 9780128166758.
3. Tamburrini, A.; Colombo, C.; Bernardi, A. Design and synthesis of glycomimetics: Recent advances. *Med. Res. Rev.* **2020**, *40*, 495–531. [CrossRef] [PubMed]
4. Sattin, S.; Bernardi, A. Design and synthesis of glycomimetics. In *Carbohydrate Chemistry*; Rauter, A.P., Lindhorst, T.K., Queneau, Y., Eds.; The Royal Society of Chemistry: Cambridge, UK, 2016; Volume 41, pp. 1–25, ISBN 978-1-78262-121-8.
5. Ernst, B.; Magnani, J.L. From carbohydrate leads to glycomimetic drugs. *Nat. Rev. Drug Discov.* **2009**, *8*, 661–677. [CrossRef] [PubMed]
6. Compain, P.; Martin, O.R. (Eds.) *Iminosugars: From Synthesis to Therapeutic Applications*; John Wiley & Sons: Chichester, UK, 2007; ISBN 978-0-470-03391-3.
7. Asano, N. Iminosugars: The Potential of Carbohydrate Analogs. In *Carbohydrate Chemistry: State of the Art and Challenges for Drug Development*; Cipolla, L., Ed.; Imperial College Press: London, UK, 2016; pp. 279–301. ISBN 978-1783267194.
8. Harit, V.K.; Ramesh, N.G. Amino-functionalized iminocyclitols: Synthetic glycomimetics of medicinal interest. *RSC Adv.* **2016**, *6*, 109528–109607. [CrossRef]
9. Conforti, I.; Marra, A. Iminosugars as glycosyltransferase inhibitors. *Org. Biomol. Chem.* **2021**, *19*, 5439–5475. [CrossRef] [PubMed]
10. Alonzi, D.S.; Scott, K.A.; Dwek, R.A.; Zitzmann, N. Iminosugar antivirals: The therapeutic sweet spot. *Biochem. Soc. Trans.* **2017**, *45*, 571–582. [CrossRef]

11. Horne, G. Alkaloids as important scaffolds in therapeutic drugs for the treatments of cancer, tuberculosis, and smoking cessation. *Top. Med. Chem.* **2014**, *12*, 23–51. [CrossRef]
12. Nicolas, C.; Engo-Ilanga, F.; Cocaud, C.; Martin, O.R. En Route to Novel Furanoside Mimics Through Stereoselective Zinc-Mediated Propargylation of *N*-Benzyl-glycofuranosylamines Using Ultrasound Activation. *Synlett* **2015**, *26*, 187–192. [CrossRef]
13. Cocaud, C.; Maujoin, A.; Zheng, R.B.; Lowary, T.L.; Rodrigues, N.; Percina, N.; Chartier, A.; Buron, F.; Routier, S.; Nicolas, C.; et al. Triazole-Linked Iminosugars and Aromatic Systems as Simplified UDP-Gal*f* Mimics: Synthesis and Preliminary Evaluation as Gal*f*-transferase Inhibitors. *Eur. J. Org. Chem.* **2017**, *41*, 6192–6201. [CrossRef]
14. Cocaud, C.; Nicolas, C.; Poisson, T.; Pannecoucke, X.; Legault, C.Y.; Martin, O.R. Tunable Approach for the Stereoselective Synthesis of 1-*C*-Diethylphosphono(difluoromethyl) Iminosugars as Glycosyl Phosphate Mimics. *J. Org. Chem.* **2017**, *82*, 2753–2763. [CrossRef]
15. Cocaud, C.; Zheng, R.B.; Lowary, T.; Poisson, T.; Pannecoucke, X.; Nicolas, C.; Martin, O.R. 1-*C*-Phosphonomethyl- and 1-*C*-Difluorophosphonomethyl-1,4-imino-L-arabinitols as Gal*f* Transferase Inhibitors: A Comparison. *Carbohydr. Res.* **2018**, *461*, 45–50. [CrossRef]
16. Nicolas, C.; Martin, O.R. Glycoside Mimics From Glycosylamines: Recent Progress. *Molecules* **2018**, *23*, 1612. [CrossRef] [PubMed]
17. Li, S.; Jaszczyk, J.; Pannecoucke, X.; Poisson, T.; Martin, O.R.; Nicolas, C. Stereospecific Synthesis of Glycoside Mimics Through Migita–Kosugi–Stille Cross-Coupling Reactions of Chemically and Configurationally Stable 1-*C*-Tributylstannyl Iminosugars. *Adv. Synth. Catal.* **2021**, *363*, 470–483. [CrossRef]
18. Chronowska, A.; Gallienne, E.; Nicolas, C.; Kato, A.; Adachi, I.; Martin, O.R. An expeditious synthesis of an analogue of (−)-steviamine by way of the 1,3-dipolar cycloaddition of a nitrile oxide with a 1-*C*-allyl iminosugar. *Tetrahedron Lett.* **2011**, *52*, 6399–6402. [CrossRef]
19. Ernholt, B.V.; Thomsen, I.B.; Lohse, A.; Plesner, I.W.; Jensen, K.B.; Hazell, R.G.; Liang, X.; Jakobsen, A.; Bols, M. Enantiospecific Synthesis of 1-Azafagomine. *Chem. Eur. J.* **2000**, *6*, 278–287. [CrossRef]
20. Yu, C.-Y.; Huang, M.-H. Radicamines A and B: Synthesis and Revision of the Absolute Configuration. *Org. Lett.* **2006**, *8*, 3021–3024. [CrossRef]
21. Liu, C.; Gao, J.; Yang, G.; Wightman, R.H.; Jiang, S. Enantiospecific Synthesis of (–)-Radicamine B. *Lett. Org. Chem.* **2007**, *4*, 556–558. [CrossRef]
22. Van Rijssel, E.R.; van Delft, P.; Lodder, G.; Overkleeft, H.S.; van der Marel, G.A.; Filippov, D.V.; Codée, J.D.C. Furanosyl Oxocarbenium Ion Stability and Stereoselectivity. *Angew. Chem. Int. Ed.* **2014**, *53*, 10381–10385. [CrossRef] [PubMed]
23. Wennekes, T.; Bonger, K.M.; Vogel, K.; van den Berg, R.J.B.H.N.; Strijland, A.; Donker-Koopman, W.E.; Aerts, J.M.F.G.; van der Marel, G.A.; Overkleeft, H.S. The Development of an Aza-C-Glycoside Library Based on a TandemStaudinger/Aza-Wittig/Ugi Three-Component Reaction. *Eur. J. Org. Chem.* **2012**, *32*, 6420–6454. [CrossRef]
24. Evangelista, T.C.S.; Lopéz, Ó.; Sydnes, M.O.; Fernández-Bolaños, J.G.; Ferreira, S.B.; Lindbäck, E. Bicyclic 1-Azafagomine Derivatives: Synthesis and Glycosidase Inhibitory Testing. *Synthesis* **2019**, *51*, 4066–4077. [CrossRef]
25. Altona, C.; Sundaralingam, M. Conformational Analysis of the Sugar Ring in Nucleosides and Nucleotides. A New Description Using the Concept of Pseudorotation. *J. Am. Chem. Soc.* **1972**, *94*, 8205–8212. [CrossRef]
26. Taha, H.A.; Richards, M.R.; Lowary, T.L. Conformational Analysis of Furanoside-Containing Mono- and Oligosaccharides. *Chem. Rev.* **2013**, *113*, 1851–1876. [CrossRef] [PubMed]
27. Groom, C.R.; Bruno, I.J.; Lightfoot, M.P.; Ward, S.C. The Cambridge Structural Database. *Acta Crystallogr. Sect. B Struct. Sci. Cryst. Eng. Mater.* **2016**, *72*, 171–179. [CrossRef] [PubMed]
28. Suthagar, K.; Polson, M.I.J.; Fairbanks, A.J. Unexpected furanose/pyranose equilibration of *N*-glycosyl sulfonamides, sulfamides and sulfamates. *Org. Biomol. Chem.* **2015**, *13*, 6573–6579. [CrossRef] [PubMed]
29. Spackman, M.A.; Jayatilaka, D. Hirshfeld Surface Analysis. *CrystEngComm* **2009**, *11*, 19–32. [CrossRef]
30. Rigaku, O.D. *CrystalClear*, version 2.0; Rigaku Corporation: Tokyo, Japan, 2008.
31. Rigaku, O.D. *CrysAlisPro*, version 1.171.41.121a; Rigaku Oxford Diffraction: Yarnton, UK, 2021.
32. Sheldrick, G.M. SHELXT—Integrated space-group and crystal-structure determination. *Acta Crystallogr. Sect. A Found. Adv.* **2015**, *71*, 3–8. [CrossRef] [PubMed]
33. Sheldrick, G.M. Crystal Structure Refinement with SHELXL. *Acta Crystallogr. Sect. C Struct. Chem.* **2015**, *71*, 3–8. [CrossRef]
34. Fugel, M.; Jayatilaka, D.; Hupf, E.; Overgaard, J.; Hathwar, V.R.; Macchi, P.; Turner, M.J.; Howard, J.A.K.; Dolomanov, O.V.; Puschmann, H.; et al. Probing the accuracy and precision of Hirshfeld atom refinement with *HARt* interfaced with *Olex2*. *IUCrJ* **2018**, *5*, 32–44. [CrossRef]
35. Kleemiss, F.; Dolomanov, O.V.; Bodensteiner, M.; Peyerimhoff, N.; Midgley, L.; Bourhis, L.J.; Genoni, A.; Malaspina, L.A.; Jayatilaka, D.; Spencer, J.L.; et al. Accurate crystal structures and chemical properties from *NoSpherA2*. *Chem. Sci.* **2021**, *12*, 1675–1692. [CrossRef]
36. Dolomanov, O.V.; Bourhis, L.J.; Gildea, R.J.; Howard, J.A.K.; Puschmann, H. *OLEX2*: A complete structure solution, refinement and analysis program. *J. Appl. Cryst.* **2009**, *42*, 339–341. [CrossRef]
37. Becke, A.D. Density-functional thermochemistry. III. The role of exact exchange. *J. Chem Phys.* **1993**, *98*, 5648–5652. [CrossRef]
38. Weigend, F.; Ahlrichs, R. Balanced basis sets of split valence, triple zeta valence and quadruple zeta valence quality for H to Rn: Design and assessment of accuracy. *Phys. Chem. Chem. Phys.* **2005**, *7*, 3297–3305. [CrossRef] [PubMed]

39. Parsons, S.; Flack, H.D.; Wagner, T. Use of intensity quotients and differences in absolute structure refinement. *Acta Crystallogr. Sect. B Struct. Sci. Cryst. Eng. Mater.* **2013**, *69*, 249–259. [CrossRef] [PubMed]
40. Spek, A.L. Structure validation in chemical crystallography. *Acta Crystallogr. Sect. D Biol. Crystallogr.* **2009**, *65*, 148–155. [CrossRef] [PubMed]